

Hot coronae in nearby radio galaxies

E. Trussoni¹, S. Massaglia², R. Ferrari², R. Fanti^{3,4}, L. Feretti⁴, P. Parma⁴, and W. Brinkmann⁵

¹ Osservatorio Astronomico di Torino, Strada dell'Osservatorio 20, I-10025 Pino Torinese, Italy

² Dipartimento di Fisica Generale dell'Università, Via P. Giuria 1, I-10125 Torino, Italy

³ Dipartimento di Fisica dell'Università, Via Imerio 46, I-40126 Bologna, Italy

⁴ Istituto di Radioastronomia del CNR, Via Gobetti 101, I-40129 Bologna, Italy

⁵ Max-Planck-Institut für Extraterrestrische Physik, Postfach 1603, D-85740 Garching, Germany

Received 14 February 1997 / Accepted 22 April 1997

Abstract. We present Rosat X-ray observations (with PSPC and HRI instruments) of a sample of radio galaxies belonging to the B2 catalog (3C31, 0206+35, 1113+29 and 1553+24). The source 3C31 (B2 0104+32) belongs to the group Arp 331 which shows emission from a diffuse hot intra-group gas and from the brightest members of the group. We discuss both the morphological and spectral features of this extended region deriving, in the framework of an isothermal beta model, the core radius, the central density, the mass of the emitting material and gravitational mass, obtaining indications on the presence of dark matter. A comparison of X-ray and radio data shows that the thermal pressure of the external gas exceeds the minimum pressure of the radio components, apart from the region close to the nucleus where the jet is over-pressured. The X-ray emission from the single members of the group and from the other galaxies of the sample are consistent with a thermal spectrum originating from hot halos, which is a common feature in early type galaxies. We discuss the main morphological and physical properties of these coronae. Furthermore, using also the data of previous works, we confirm the strong correlation between the X-ray and optical luminosities of all these galaxies.

Key words: galaxies: intergalactic medium – galaxies: jets – radio continuum: galaxies – X-rays: galaxies

1. Introduction

The discovery of X-ray emitting hot coronae and intracluster gas by the Einstein satellite has allowed a significant improvement in the understanding of the physical properties of galaxies.

Most important for its cosmological implications was the discovery of dark matter in groups and clusters. Moreover, the evolution of radio sources on small and large scales is critically governed by the interaction of the emitted plasmoids or jets with

the external hot plasma. Among these effects one can recall the confinement and stability of jets, the entrainment of external gas, and the onset of terminal and internal shocks where particle acceleration may occur (Fanti 1984, Burns 1986, Bicknell et al. 1990). The theoretical modeling of these processes requires the knowledge of the physical parameters of the radio emitting plasma (deduced from radio observations) and of the hot external gas (obtained from X-ray data).

One of the most relevant results of X-ray observations of the ambient medium that surrounds low brightness sources is that the radio emitting components seem to have a minimum pressure lower than the external hot gas (see Morganti et al. 1988, Feretti et al. 1990, 1992). This trend has been recently confirmed by Rosat observations of a small sample of low brightness radio galaxies of the B2 catalog (1615+35, 1621+38, Feretti et al. 1995; 1122+39, Massaglia et al. 1996).

We present here, in the same scheme, the results of Rosat pointed observations of the radio galaxies 3C31 (B2 0104+32), B2 0206+35, B2 1113+29 and B2 1553+24. The radio sources 3C31 and 0206+35 have been observed with both the Position Sensitive Proportional Counter (PSPC) and the High Resolution Imager (HRI), while for the two last objects we have data from the HRI only. Besides 0206+35, the other radio galaxies have been observed with the Einstein observatory by Morganti et al. (1988), who have first shown that radio blobs exist with pressure lower than the external one.

The outline of this paper is the following. In Sect. 2 we recall the main results obtained from previous observations of these sources in X-rays and at other wavelengths; in Sect. 3 we report the details of the present observations and the data analysis. In Sect. 4 we discuss results from the morphological and spectral analysis for all the sources, while in Sec. 5 we deduce and discuss the relevant physical parameters and their interpretation, including also the results obtained in our previous published papers. The results are summarized in Sec. 6.

A Hubble constant $H_0=50 \text{ km s}^{-1} \text{ Mpc}^{-1}$ is used throughout the paper.

Send offprint requests to: E. Trussoni

Table 1. Source parameters

Name	z	R.A. (2000)			DEC			m _B	S _{1.4} mJy	LAS ^a "
		h	m	s	°	'	"			
3C31	0.0169	01	07	24.0	32	24	36	13.4	5280	1500
B2 0206+35	0.0375	02	09	38.3	35	48	00	14.3	2050	89
B2 1113+29	0.0489	11	16	33.6	29	15	00	15.1	1810	91
B2 1553+24	0.0426	15	56	04.8	24	26	00	15.4	124	55

^aLargest Angular Size at 1.4 GHz

Table 2. Observational details

Name	Instrument	Date	Exposure (s)
3C31	PSPC	Jul 91	29,430
	HRI	Jan 92	2,765
B2 0206+35	PSPC	Jul 92	14,843
	HRI	Feb 94	21,590
B2 1113+29	HRI	May/Jun 92	6,547
B2 1553+24	HRI	Mar 94	8,466
	HRI	Aug 94	20,559

2. The sources

We recall here the main features of the objects under study. The source data are given in Table 1.

2.1. 3C31 (B2 0104+32, NGC 383)

The radio source 3C31 is associated with the galaxy NGC 383, the brightest member of the the group (chain) Arp 331, in the Perseus-Pisces super-cluster, comprising NGC 379, NGC 380, and NGC 382-386 (NGC 382 is at $\approx 35''$ from NGC 383 in the SW direction). The galaxy shows a dust lane at $\approx 3.7''$ from the central region (Fraix-Burnet et al. 1991) and is also an infrared source with a total luminosity in the range $10 - 100\mu\text{m}$ of $L_{\text{IR}} \approx 8 \times 10^{43} \text{ erg s}^{-1}$ (Impey, Wynn-Williams & Becklin 1990).

At radio wavelengths, 3C31 is an intermediate luminosity source ($P_{1.4\text{GHz}} \approx 10^{24} \text{ W Hz}^{-1}$) that shows two prominent radio jets emerging from a central unresolved core, for a total extent of $\approx 25'$ ($\approx 750 \text{ kpc}$, see Strom et al. 1983).

Observations with the IPC detector of the Einstein satellite provided quite detailed data on the hot gas surrounding the galaxy (Morganti et al. 1988). In the HRI, an unresolved source was detected coincident with the galactic nucleus and the radio core.

2.2. B2 0206+35 (4C 35.03)

The elliptical galaxy associated to this source (UGC 1651) belongs to the Zwicky cluster 0216.0+3625. The two radio jets emerging from the nucleus, have at 1.4 GHz an extension of $\approx 35''$ ($\approx 40 \text{ kpc}$) in the NW - SE direction. They appear to be embedded in a weaker diffuse radio emission of total extent $\approx 1.5'$ ($\approx 100 \text{ kpc}$; Parma et al. 1987, Morganti et al. 1987). At X-ray frequencies a point-like source plus extended emis-

sion has been detected from a pointed Rosat/PSPC observation (Worrall & Birkinshaw 1994).

2.3. B2 1113+29

This radio source (also known as 4C29.41) is associated to the galaxy CGCG 156-046 belonging to a double system of galaxies close to the center of the cluster Abell 1213. At radio frequencies it shows a double structure with total size $\approx 120 \text{ kpc}$ with a one-sided jet of length $\approx 45 \text{ kpc}$ (Fanti et al. 1986). An extended weak X-ray emission associated to the cluster has been detected in the IPC of Einstein (Morganti et al. 1988).

2.4. B2 1553+24

The radio source is associated to the galaxy CGCG 137-003, which has been found to show H_{α} emission in the central region (Morganti et al. 1992). At radio frequencies two twin 'naked' jets of size $\approx 30 \text{ kpc}$ emerge from the core (Parma et al. 1987). A weak extended X-ray emission has been detected by the Einstein-IPC (Morganti et al. 1988).

3. Observations and data reduction

The observations were performed with the ROSAT HRI and PSPC detectors (see Trümper 1983, and Pfeffermann et al. 1987). The data analysis has been carried out employing the January 1996 release of the Exsas package (Zimmermann et al. 1995). The observation of 3C31 (PSPC and HRI) and 0206+35 (PSPC) have been extracted from the public archive, while the other pointed observations were proposed by the authors.

All the data have been corrected for vignetting and dead-time, and the contamination from high energy particles has been removed. To avoid too high background towards the end of each orbital transit, the PSPC exposure of 3C31 has been reduced to 25,756 s.

The background has been extracted from annuli centered on the target position, with size depending on the source extent. In the PSPC observation of 3C31 the outer region of the diffuse emission of size $\sim 0.6^{\circ}$ is masked by the detector supports. In such a case the background has been selected from a circular corona with internal and external radius 4,500 and 6,000 pixels, respectively, removing the 'dead' regions hidden by the support structure of the PSPC.

For the spectral analysis, only the channels 11 - 235 of the PSPC were considered, corresponding to an energy range 0.15 - 2.1 keV. The errors reported in the text for the parameters

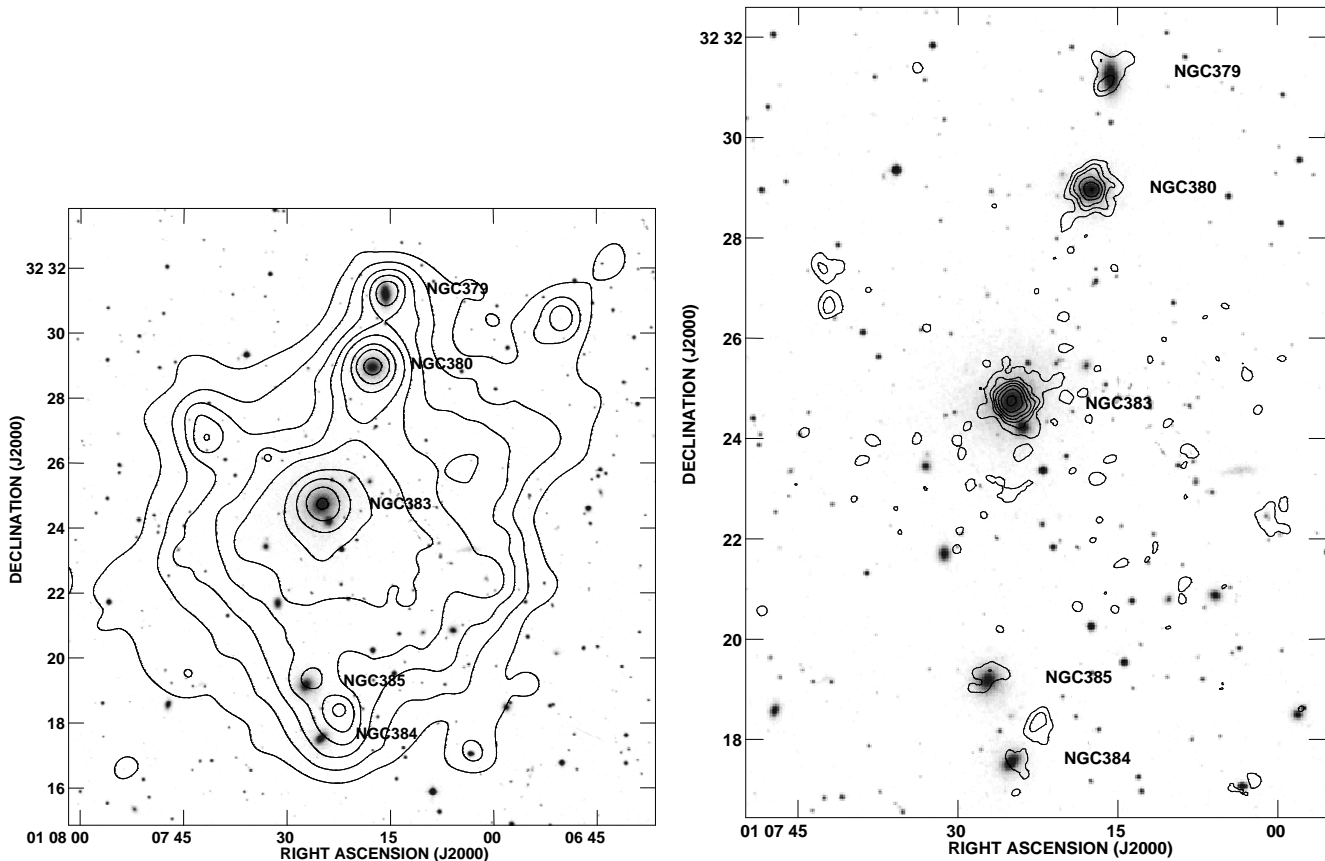


Fig. 1. *Left:* Overlay of the PSPC X-ray contours onto the grey-scale image of the optical (red) plate of 3C31 (B2 0104+32). The X-ray map has been smoothed with Gaussians of increasing width with decreasing count rate up to $\sim 3'$ (FWHM), to enhance the low brightness structures. Contours are at 64, 66, 68, 69, 70, 73, 75, 81, 94% of the peak of $3.71 \text{ counts pixel}^{-1}$ (1 pixel = $4.5'' \times 4.5''$). The first contour corresponds to a level of about 3σ above the background. Sources are labeled according to Table 1 (in this and the following figures the coordinates are at J2000). *Right:* The same as in the left panel, showing the X-ray emission of the galaxies of the chain Arp 331, smoothed with a Gaussian of $30''$ (FWHM). Contours are 9, 15, 21, 30, 42, 61, 91% of the peak emission of $1.65 \text{ counts pixel}^{-1}$ (1 pixel = $2'' \times 2''$)

obtained from the spectral fits are at 68% confidence values. The positional errors in the PSPC and HRI maps have been corrected by overlaying the X-ray maps on the optical plates.

The observational details for each source are summarized in Table 2, while the main X-ray data, with the corresponding count rates, are reported in Table 3.

The optical maps have been extracted from the digitized Palomar Sky Survey (PSS).

4. Results

4.1. 3C31 group

X-ray emission has been detected in the PSPC from the five most luminous galaxies of the chain Arp 331. These sources are embedded in a region of diffuse emission which extends beyond the ring-like support of the detector. The X-ray contour maps showing the diffuse region and the emission from the single galaxies of the chain are shown, overlaid to the optical plates of the same region, in Fig. 1.

With the HRI detector, emission has been detected from NGC 383 and NGC 380 only, due to the short observation.

4.1.1. Diffuse component

The diffuse component detected with the PSPC shows an approximate radius of $\approx 17'$ (corresponding to a total extension of $\approx 1 \text{ Mpc}$) with an emission peak at $\approx 1.5'$ southwards from the center of NGC 383.

The spectrum of the diffuse component has been fitted to an optically thin plasma model (Raymond & Smith 1977; see Fig. 2). The results of the spectral analysis are summarized in Table 4. The parameters are obtained by fixing the hydrogen column density to the Galactic value. By leaving the hydrogen column density as a free parameter, we obtain $N_{\text{H}} = 6.6_{-1.1}^{+2.0} \times 10^{20} \text{ cm}^{-2}$, consistent within the errors with the Galactic absorption, a temperature $kT = 1.46_{-0.10}^{+0.08} \text{ keV}$ and a metallicity (with respect to the standard cosmic value) $\mathcal{M} = 0.36_{-0.13}^{+0.15}$.

In order to check the degree of homogeneity in temperature of the diffuse emission we have verified that fits to the flux

Table 3. Detected sources

Source	R.A. (2000)			DEC			$N_{\text{H,gal}}$ $\times 10^{20} \text{ cm}^{-2}$	CR_{PSPC} $\times 10^{-2} \text{ s}^{-1}$	CR_{HRI} $\times 10^{-3} \text{ s}^{-1}$	Size (FWHM) "
	h	m	s	°	'	"				
Diffuse 3C31	01	07	23.1	32	22	59	5.23	43.0 ± 9.0		710
NGC 383 (3C31)	01	07	24.8	32	24	52	5.23	1.90 ± 0.13	6.3 ± 1.7	<5
NGC 379	01	07	15.7	32	31	24	5.36	0.39 ± 0.06		<25
NGC 380	01	07	17.5	32	29	09	5.36	1.20 ± 0.10	5.9 ± 2.4	<5
NGC 384	01	07	22.8	32	17	50	5.23	0.15 ± 0.03		<25
NGC 385	01	07	26.7	32	19	22	5.23	0.23 ± 0.04		<25
B2 0206+35	02	09	38.6	35	47	50	5.84	2.1 ± 0.3	6.6 ± 1.2	< 25 ^a
B2 1113+29	11	16	34.5	29	15	11	1.59		2.0 ± 0.6	<5
B2 1553+24	15	56	3.9	24	26	53	4.47		3.0 ± 0.4	4.5

^a The compact source is surrounded by an extended region of size $\approx 160''$

from the inner (circle with radius $\approx 8'$) and outer zone (circular corona within $\approx 8' - 17'$) lead to a temperature consistent with that deduced considering the whole region. This is confirmed by a fit with a two-temperature thermal spectrum that has revealed no evidence of a second thermal component.

To test the matter distribution within the group, we have analyzed the fluxes selected from four circular regions of radius $\approx 6.5'$, with the center at $\approx 12'$ and in the NE, NW, SW and SE directions from the central emission peak. The values of N_{H} and \mathcal{M} are different in the various sectors, but always within the statistical errors, except in the NW region where we find $N_{\text{H}} \gtrsim 9 \times 10^{20} \text{ cm}^{-2}$ at 99.7 % confidence level. The low quality of the fits does not allow further discussion, however the origin of this extra absorption is not clear. One possibility could be the mixture of components at different temperatures. For the purposes of the present study, we will consider the whole region of diffuse emission with the spectral parameters obtained assuming $N_{\text{H}} = N_{\text{H,gal}}$. The total flux is given in Table 5.

A radial profile of the brightness distribution of the extended region has been obtained by integrating the counts over annuli of $30''$ of size, centered on the approximate X-ray centroid. The radial profile was fit to an hydrostatic isothermal model, described by the functional form (Cavaliere & Fusco-Femiano 1981, Sarazin 1986):

$$I(r) = I_0(1 + r^2/r_c^2)^{-3\beta+0.5}$$

where I_0 is the central surface brightness, r_c is the core radius, and β is the ratio between kinetic energy of the galaxies and the thermal energy of the gas. The background is also fit and the instrument point spread function is taken into account. The parameters obtained from the fit are: $I(0) = 4.6 \times 10^{-7} \text{ cts s}^{-1} \text{ arcsec}^{-2}$, $\beta = 0.61 \pm 0.06$ and $r_c = 460'' \pm 60''$, with a reduced $\chi^2 \approx 4$. The diffuse emission, which appears quite isotropic, extends up to $\approx 3r_c$, so that it is partially obscured

by the ring-like detector support, preventing the achievement of a better fit. Following Feretti et al. (1995) the values of β and r_c allowed us to derive the central density value of the emitting gas of the extended component, $n_c \simeq (6.5 \pm 0.3) \times 10^{-4} \text{ cm}^{-3}$. The mass of emitting gas, within one core radius, turns out to be $M_{\text{gas}} \simeq 3.5 - 6 \times 10^{11} M_{\odot}$.

4.1.2. Emission from the galaxies of the chain Arp 331

The radial count rate distribution for NGC 383 is basically consistent with the point spread function of both PSPC and HRI instruments. Keeping the hydrogen column density fixed to its Galactic value $N_{\text{H,gal}}$, the flux is consistent with a thermal Raymond-Smith spectrum (see Table 4 and Fig. 3). A power-law spectrum does not fit the data, however a non-thermal fraction from a point-like central source cannot be excluded. Fixing the photon index of the non-thermal component ($\alpha = -1.9$), its contribution to the total flux increases from $\sim 25\%$ to $\sim 60\%$ for $\mathcal{M} = 0.1 \rightarrow 1$. The large statistical errors do not allow a more detailed spectral analysis.

With the parameters deduced from the PSPC data, we expect in the HRI a count rate $\approx 7 \times 10^{-3} \text{ s}^{-1}$, which is consistent with the observed photon flux. Even though not yet conclusive, due to the very short exposure (18 photons detected), these data imply small dimensions for the emitting region ($\lesssim 5''$).

The PSPC radial profile for NGC 380 is consistent with the point spread function of the detector. The spectral analysis provides results quite similar to those obtained for NGC 383: the flux is consistent with a thermal emission (see Table 4 and Fig. 3), with a possible contribution from a non-thermal component. The fit to a power-law spectrum is not acceptable, as expected for a radio quiet object.

In the short HRI exposure the brightness profile is typical for a point-like source, with the count rate as expected from the

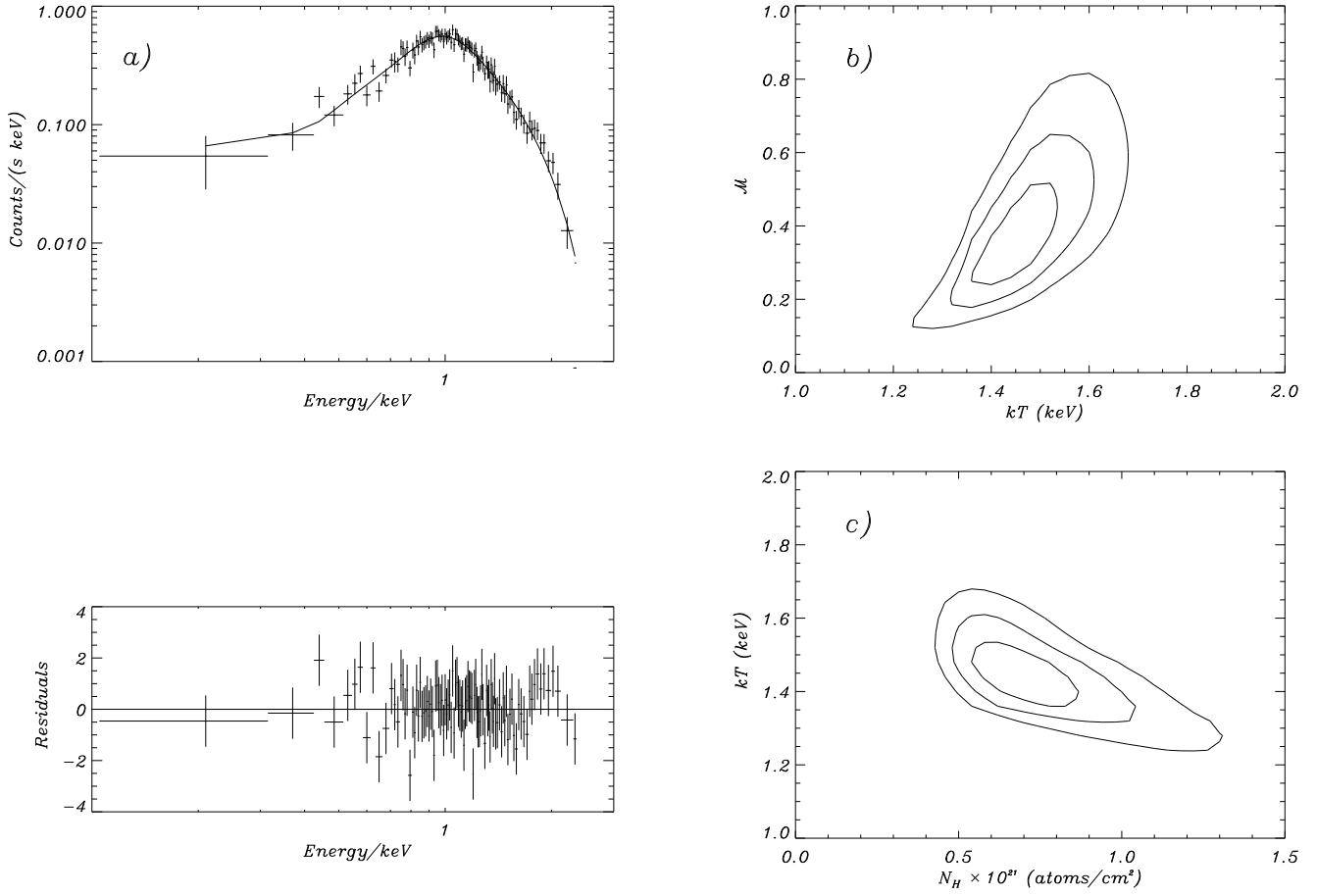


Fig. 2. **a** Spectrum of the diffuse source surrounding 3C31 and the chain Arp 331 assuming an optically thin thermal plasma spectrum. **b** Confidence levels at 68%, 95% and 99% of the metallicity \mathcal{M} versus the temperature kT . **c** The same as in panel **b** for the temperature kT versus the hydrogen column density N_{H}

Table 4. X-ray parameters for thermal model

Source	kT keV	\mathcal{M}	$\chi^2/(d.o.f.)$	Factor/ 10^{-11} erg cm $^{-2}$ ct $^{-1}$	$F_{\text{X}}/10^{-13}$ ^a erg cm $^{-2}$ s $^{-1}$
Diffuse 3C31	$1.50^{+0.08}_{-0.11}$	$0.48^{+0.15}_{-0.11}$	0.8 (99)	1.84 (PSPC)	79.1
3C31	$0.80^{+0.15}_{-0.15}$	$0.08^{+0.08}_{-0.03}$	0.7 (16)	1.66 (PSPC)	3.15
NGC 379	$0.57^{+0.30}_{-0.28}$	$\gtrsim 0.04$	1.4 (7)	1.69 (PSPC)	0.66
NGC 380	$0.90^{+0.14}_{-0.15}$	$0.22^{+0.78}_{-0.12}$	0.7 (11)	1.58 (PSPC)	1.9
NGC 384	0.9 ^b	0.2 ^b		1.59 (PSPC)	0.24
NGC 385	0.9 ^b	0.2 ^b		1.59 (PSPC)	0.37
B2 0206+35	$1.27^{+0.83}_{-0.30}$	$\gtrsim 0.03$	0.7 (11)	1.60 (PSPC)	3.37
B2 1113+29	1 ^b	0.5 ^b		3.08 (HRI)	0.62
B2 1553+24	1 ^b	0.5 ^b		3.56 (HRI)	1.07

^a Energy band: 0.1 - 2.4 keV ^b Assumed values

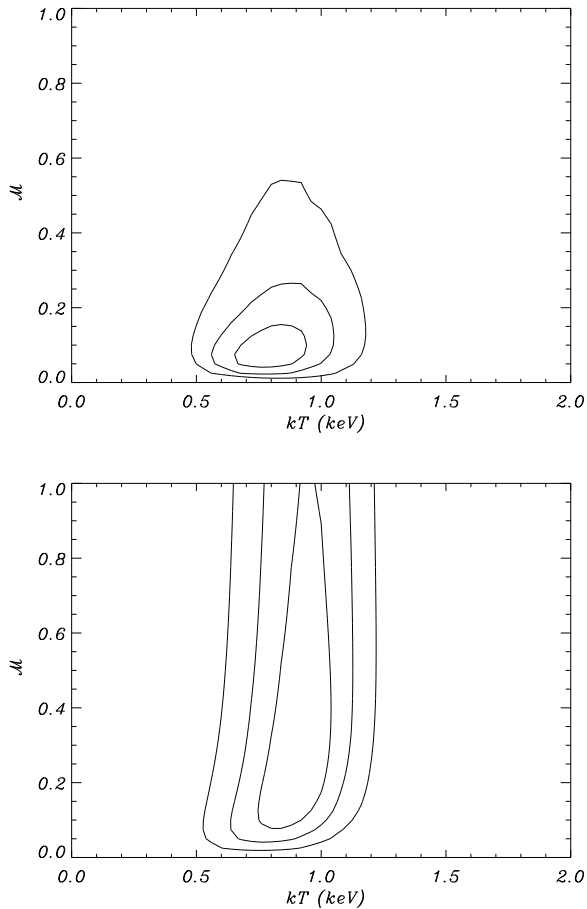


Fig. 3. Above: Confidence levels at 68%, 95% and 99% of the metallicity \mathcal{M} versus the temperature kT (with $N_{\text{H}} = N_{\text{H,gal}}$) for NGC 383 assuming an optically thin thermal plasma spectrum. Below: The same as in the upper panel for NGC 380

PSPC observation. Therefore also for NGC 380 the dominant emission is thermal and quite concentrated towards the galactic center.

The weak emission from NGC 379, NGC 385 and NGC 384 does not allow a useful determination of the spectral parameters (see Table 4). For NGC 379 only, we can have an estimate of the temperature and a lower limit for the metallicity. For the computation of flux and luminosity, we assumed the parameters derived for NGC 380.

4.2. B2 0206+35

We have reanalyzed the PSPC observation presented by Worrall & Birkinshaw (1994), using also the information derived from the HRI data. The contour maps of the PSPC X-ray image of B2 0206+35 and the overlay of the X-ray map on the radio image are presented in Figs. 4: the compact central source, consistent with the PSF, is surrounded by an extended halo of very low brightness (radius $\approx 2.5'$).

In the HRI only the central compact region is detected, with a count rate lower by a factor ≈ 2.5 than the photon flux detected

in the PSPC observation. The source appears extended (radius $\approx 30''$), however, an inspection of the HRI pointing stability implies that the attitude errors can be quite larger than expected. Therefore it is not possible to say whether this region is actually extended or point-like.

This complex structure is not consistent with a simple hydrostatic model. In Worrall & Birkinshaw (1994) the extended emission was fitted to a beta model with $r_c \approx 70$ kpc, assuming $\beta = 0.67$. This value of the core radius is much higher than found in similar objects (see e.g. Feretti et al. 1995, Massaglia et al. 1996), therefore we cannot exclude a contribution from an intra-group plasma to the X-ray emission from the galactic atmosphere. It is also worth noticing that there is a weak narrow tail of emission in the E direction ($\sim 4\sigma$ above the background, See Fig. 4).

Due to the low count rate and the extension of the source, very little information can be obtained from the spectral analysis. The detected emission is consistent with both a thermal and a non-thermal spectrum; Worrall & Birkinshaw (1994) fit the data to a two component spectrum (thermal + power law), but without a useful determination of the parameters.

If the total emission from the inner and outer regions originates from a hot plasma, the spectral analysis yields a somewhat high temperature for a hot corona (see Table 4). Conversely, one expects a non-thermal spectrum if the emission detected in the HRI is point-like and associated to a compact source in the galactic center. Assuming a two component spectrum, with the same parameters for the thermal spectrum as in Table 4, and fixing $\alpha = -1.9$ for the power law spectrum, we deduce $F_{\text{th}} = 1.6 \times 10^{42}$ erg s $^{-1}$ and $F_{\text{pl}} = 2.0 \times 10^{42}$ erg s $^{-1}$, consistent with Worrall & Birkinshaw (1994).

4.3. B2 1113+29

This source appears point-like in the HRI. The X-ray emission could be of non-thermal origin, associated with the active nucleus. However, given the short exposure, we cannot exclude that the X-ray emission is the tip of a gaseous extended atmosphere. The flux and luminosity have been evaluated assuming thermal emission.

4.4. B2 1553+24

The HRI map of 1553+24 is given in Fig. 5. The X-ray emission appears elongated in the direction of the galaxy optical minor axis. A brightness radial profile was obtained by integrating in concentric annuli of $5''$ around the X-ray peak. A fit of the radial profile to the hydrostatic isothermal model does not give reliable results, probably because of the asymmetry in the brightness distribution. By comparing the source profile with the PSF, we evaluated that the source size is $\approx 4.5''$, with the contribution of a possible point-like component to the total count rate of $\lesssim 45\%$. The same spectral parameters as in B2 1113+29 have been assumed to evaluate the luminosity.

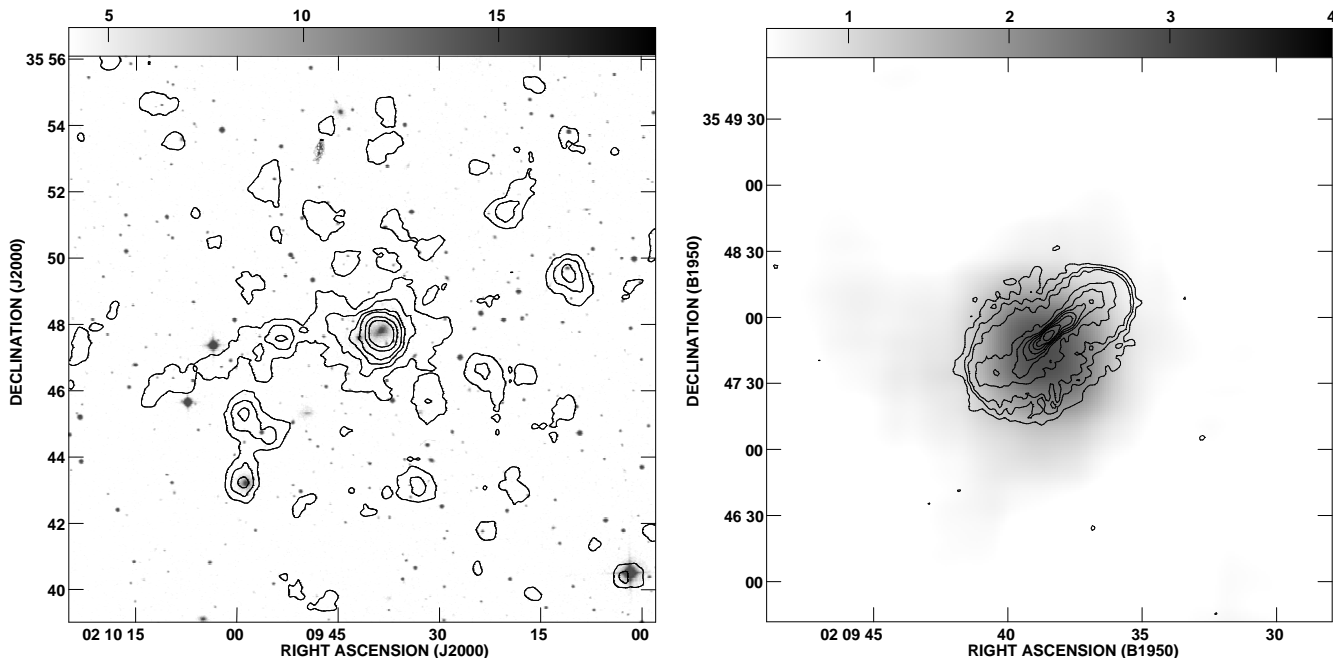


Fig. 4. *Left:* Overlay of the PSPC X-ray contours onto the grey-scale image of the optical (red) plate of B2 0206+35. The X-ray map has been smoothed to a Gaussian of $55''$ (FWHM). Contours are at 13, 20, 27, 34, 51, 68% of the peak of $6.23 \text{ counts pixel}^{-1}$ (1 pixel = $7.5'' \times 7.5''$). *Right:* Overlay of the radio contour map onto the grey-scale PSPC image. The radio image was obtained with the Very Large Array at 1.4 GHz, with angular resolution of $1.5''$ (Parma et al., unpublished). Contour levels are 0.6, 1.8, 3, 6, 10, 14, 20, 30, 40, 80 mJy/beam

5. Discussion

5.1. Hot coronae

It is now well established that elliptical galaxies have hot coronae ($T \approx 10^7 \text{ K}$) which emit at X-ray frequencies (see, e.g.: Fabbiano 1989 and references therein). The relationship between X-ray and optical luminosities has been studied by many authors (e.g., Donnelly et al. 1990). Here we examine this relationship for the objects studied by us: in total we have 12 ellipticals, 8 of which are radio loud, considering also the objects analyzed in Feretti et al. (1995) and Massaglia et al. (1996).

For NGC 6109 (B2 1615+35), which in Feretti et al. (1995) was assumed non-thermal due to its point-like radial distribution of counts (in the HRI) we assumed the same parameters of B2 1113+29 and B2 1553+24. The whole flux from B2 0206+35 has been considered to be of thermal origin, neglecting the possible small contribution from the intra-group medium.

The comparison of the $L_X - L_B$ relationship for our objects with those in the literature, obtained essentially for radio quiet ellipticals, may give some clues as to whether the X-ray emission of our radio loud ellipticals is mostly thermal or non-thermal. In Fig. 6 we plot L_X versus M_{BT}^0 assuming the distances from Lynden-Bell et al. (1988), here after referred as 7S, and the B_T^0 magnitudes from the 7S or from the Third Revised Catalogue (3RC, de Vaucouleurs et al. 1991). The magnitudes from the two catalogues are in quite good agreement, except for NGC 6107, for which the 7S magnitude is brighter than that from the 3RC by about one magnitude. In this case we have chosen the 7S magnitude, which is more recent. For B2 1113+29 we used the

Zwicky magnitude corrected to B_T^0 following the prescriptions given in the 3RC. Our best fit gives:

$$\log L_X = -1.0 M_{\text{BT}}^0 + 19.4 \quad (1)$$

with a regression coefficient $r = 0.96$. We remark the agreement between our relationship and that of Donnelly et al. (1990), where L_X is in the 0.5 - 4.5 keV energy band: the spread of our data around their relationship ($\leq 0.25 \text{ dex}$) is even smaller than the scatter found by these authors (0.35 dex). This further points towards a thermal origin for most of the X-ray emission for our loud ellipticals (it is worth noticing that the 4 radio quiet galaxies of our sample do not differ from the 8 radio loud).

The core radii for the galaxies of the sample have been derived for the extended objects from the fit to the hydrostatic isothermal model. For the unresolved sources, upper limits have been estimated from the PSF. We obtain core radii of the order of a few kpc (see Table 5), with a possible correlation with absolute optical magnitude.

The central gas densities have been evaluated using the parameters of the hydrostatic isothermal model, when available, or the luminosity in the other cases. Values up to 0.1 cm^{-3} have been found.

The metallicity in the galactic atmospheres discussed here is quite low. Even if we can in principle accept values up to 1, the most likely values for most sources seem to be $\lesssim 0.2$ of the standard cosmic abundances.

Table 5. Intrinsic parameters

Source	Dist. M_B Mpc	$L_X/10^{41}$ ^a erg s ⁻¹	r_c kpc	n_0 cm ⁻³	Cluster code ^b
Diffuse	103 -	99.2	230	6.5×10^{-4}	1
3C31	103 -22.07	3.95	<2	>0.1	1
NGC 379	103 -21.44	0.83	-	-	1
NGC 380	103 -21.67	2.38	<2	>0.1	1
NGC 384	103 -21.24	0.30	-	-	1
NGC 385	103 -21.45	0.46	-	-	1
B2 0206+35	224 -23.01	21.2	<18	>0.02	1
B2 1113+29	260 -22.54	6.67	<5	>0.05	2
B2 1122+39	40 -21.17	0.76	1.3	0.09	0
B2 1553+24	296 -22.32	8.73	3.6	0.07	1
NGC 6107	189 -22.83	13.2	4.1	0.049	2
B2 1615+35	189 -22.27	2.71	<3.1	>0.05	2
B2 1621+38	189 -22.98	24.1	3.2	0.051	1

^a Energy band: 0.1 - 2.4 keV ^b Environment of the source: 0=isolated, 1=group, 2=cluster

5.2. Hot gas in poor groups

With the present data we detect the diffuse X-ray emission from the intergalactic gas in the group of 3C31, with a much larger size than previously imaged by the IPC on board the Einstein Observatory.

The physical parameters (temperature, density, brightness profile) for the intra-group plasma of the extended diffuse region are basically consistent with the properties of other objects of the same class. However, referring in particular to the group of 1615+35 (Feretti et al. 1995), we notice that the metallicity here is higher by a factor $\sim 2 - 3$. The metallicity of the ambient gas in the group of 3C31 is higher than that of the individual galaxies belonging to the group, but still consistent within the errors except for NGC 383. However this discrepancy can be overcome if a small non-thermal contribution to the thermal flux is present. We also point out that the structure of the X-ray emitting region of the 3C31 group is quite symmetric, contrary to the distribution of galaxies in the Arp 331 chain.

5.3. Implications on the dark matter

The potential well which maintains in hydrostatic equilibrium the hot isothermal intracluster gas implies a binding mass within

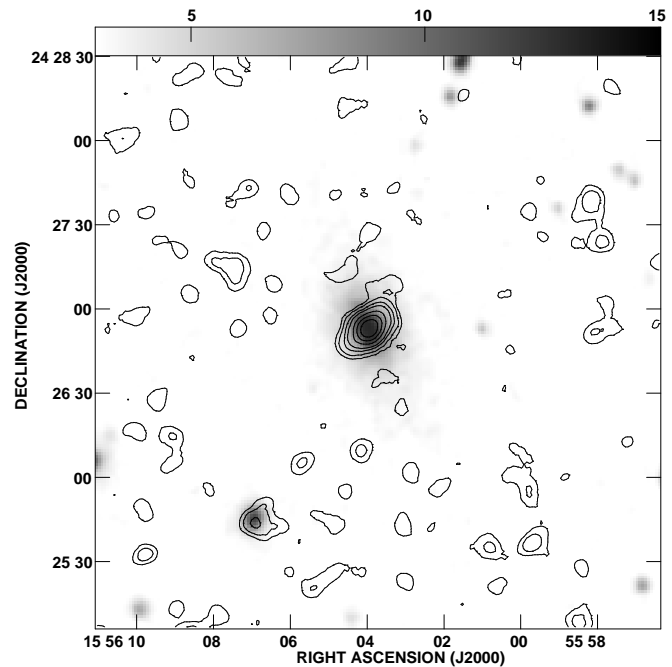


Fig. 5. Overlay of the HRI X-ray contours onto the grey-scale image of the optical (red) plate of B2 1553+24. The X-ray map has been smoothed with a Gaussian of 7'' (FWHM). Contours are at 11, 16, 24, 32, 48, 65, 81% of the peak of 0.62 counts pixel⁻¹ (1 pixel = 1'' \times 1'')

the core radius:

$$\frac{M_{grav}}{M_{\odot}} \approx 5.7 \times 10^{10} \beta \left(\frac{T}{10^7 \text{K}} \right) \left(\frac{r_c}{1 \text{Kpc}} \right) \\ \approx 1.3 - 1.9 \times 10^{13}.$$

Such value exceeds by a factor 25 - 30 the total mass of the X-ray emitting plasma obtained in Sec. 4.1.1. This implies the presence of a large amount of dark matter in the diffuse component, as found in other similar objects (Mulchaey et al. 1993, Ponman & Bertram 1993, Ponman et al. 1994, Feretti et al. 1995¹).

The lack of constrained morphological parameters does not allow in general a useful evaluation of the masses of the galactic coronae of the present sample. For NGC 383 and NGC 380, assuming a beta profile with $n_c = 0.1 \text{ cm}^{-3}$, $r_c = 2 \text{ kpc}$ and an outer radius of 10 kpc (see Table 5), and fixing $\beta = 0.6$, we obtain $M_{gas} \sim 10^9 M_{\odot}$. With these parameters we can also deduce $M_{grav}/L_B \sim 3$ (NGC 383) and ~ 9 (NGC 380). Even taking into account the large uncertainties of the parameters, we remark that the quite low value of the mass/luminosity ratio for NGC 383 could further suggest a small non-thermal contribution from the nucleus to the total X-ray luminosity. For NGC 380 conversely some amount of dark matter could be present.

We could follow the same method for the inner compact region of B2 0206+35 assuming $n_c = 0.02 \text{ cm}^{-3}$, $r_c = 18 \text{ kpc}$ and $\beta = 0.6$, but we do not know the extension of the corona,

¹ In Eq. (4) of that article it should be $\Sigma_1(x) \rightarrow \Sigma_1(x, \beta/2)$

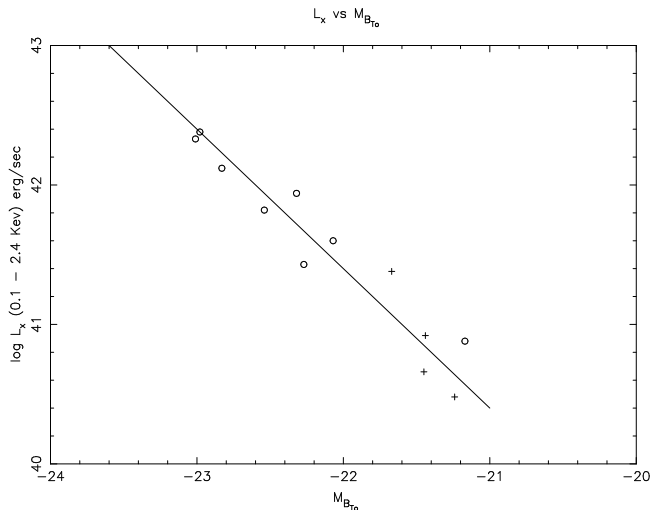


Fig. 6. Plot of the X-ray luminosity (0.1 - 2.4 keV) versus the B optical magnitude for the galaxies of the present sample. The circles refer to radio emitting galaxies, while crosses represent radio quiet ellipticals. The continuous line represents the best fit to the data (Eq. 1)

that merges into the wider diffuse region. As a lower limit, we can estimate the mass inside the assumed core radius: from the above data we obtain $M_{\text{gas}} \sim 8 \times 10^9 M_{\odot}$ and $M_{\text{grav}}/L_B \sim 4$. These values imply that either there is a large amount of dark matter in the halo or the core radius is much lower than the assumed upper limit.

5.4. Radio source confinement

For radio galaxy 3C31 where the extended gaseous emission can be fit by a hydrostatic isothermal model, we can obtain the radial profile of the pressure of the ambient gas, and compare it with the internal pressure obtained from the radio data. In Fig. 7, we show the comparison between the pressure of the ambient gas and the internal radio pressure computed from Strom et al. (1983) assuming standard equipartition conditions (with $k = 1$ and $\Phi = 1$, see Feretti et al. 1995). At distances larger than $\sim 100''$ from the core, the external pressure is larger than the minimum equipartition pressure by a factor of 2 to 6, increasing with distance. A discrepancy of a factor of 2 can be accepted as due to the errors; furthermore we must take into account possible projection effects, quite effective far from the nucleus. However it is very likely that at larger distances from the core the imbalance is significant, as already found in other sources. Conversely, the jets in their innermost regions seem not to be confined by the intracluster gas, having a minimum internal pressure $\sim 5 - 6$ times larger than that of the outer medium. This could imply that the innermost jets are confined by the galactic atmosphere, which is somewhat more extended than the size detected by the short HRI exposure. The trend observed in this source is common to the regions of low brightness in the other radio galaxies studied so far. It is likely that the difference between internal and external pressure is due to the numerous

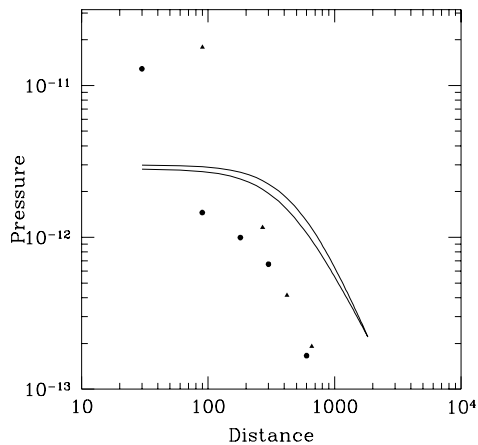


Fig. 7. Plot of the equipartition radio pressure (dots, southern jet, and triangles, northern jet) and of the allowed range of values for the thermal pressure of the X-ray emitting gas in the extended region of 3C31 (solid lines) versus the radial distance from the peak of X-ray emission. The pressure is in dyne cm^{-2} , the distance in arcsec

assumptions used for the calculation of equipartition parameters, or to the presence of thermal plasma within the radio lobes.

5.5. Non-thermal component

From the present data, and those of the other B2 radio galaxies previously studied by us, the existence of possible central unresolved sources of non-thermal origin is inferred. For this component, we generally evaluate an upper limit to the count rate from the X-ray profile, and then an upper limit to the luminosity, using a power law spectrum with photon index $\alpha = -1.9$. These upper limits are consistent with the correlation found by Worrall and Birkinshaw (1994) between the luminosity of the unresolved X-ray component and the core radio emission. This reinforces the hypothesis that a contribution from a point-like source may be present in the radio galaxies, which may be associated with the inner radio jet. However, we cannot put better constraints on this correlation, since we cannot estimate the exact contribution of this component. Furthermore, we note that the correlation of the radio versus non-thermal X-ray luminosities from the core could be affected by strong local absorption (see e.g. Makishima et al. 1994). Data at higher energies are necessary for an improved analysis.

6. Conclusions

We have analyzed the X-ray properties of a sample of low luminosity radio galaxies, and the main results can be summarized as follows:

1. The chain Arp 331 is embedded in an extended X-ray thermal emission ($kT \approx 1.5$, $\mathcal{M} \approx 0.5$), with a luminosity peak not far from the radio galaxy NGC 383 (3C31). The brightness profile is consistent with an isothermal distribution, and the mass of the

gas results to be quite lower than the binding mass. Therefore a large amount of dark matter must be present in the group.

2. Consistent with previous results, the pressure of the hot external gas is larger than the pressure inside the radio components, along almost the whole length of the lobes. However very close to the central nucleus the jet is over-pressured by a factor $\approx 6-7$.

3. The brightest members of the chain Arp 331 have X-ray emission fitted to thermal spectra (temperatures $\approx 0.6 - 0.9$ keV), that are likely to be associated with galactic coronae. The image of NGC 383 appears point-like in the HRI observation. However the higher pressure of the radio jet in its central region suggests the possible presence of an atmosphere, not detected in the very short HRI exposure. Furthermore a slight non-thermal contribution from the nucleus of NGC 383 cannot be excluded.

4. In the HRI, the X-ray emission from B2 1113+29 and B2 1553+24 come from quite compact regions, suggesting small sizes for their hot coronae (however we should not forget the short exposure for the first source).

5. The structure of B2 0206+35 is quite peculiar: a central compact region surrounded by an extended corona, much wider than expected for this class of objects. The central emission region could be associated to a galactic atmosphere, that merges into the more extended intra-group hot gas.

6. For all the 12 galaxies of our sample, including also those studied in Feretti et al. (1995) and Massaglia et al. (1996), the X-ray emission is consistent with a thermal spectrum and strongly correlated with the optical (blue) luminosity. This correlation holds for both radio loud and radio quiet galaxies.

Acknowledgements. We wish to thank C. Izzo and S. Döbereiner for their help and suggestions in the data reduction

References

- Bicknell, G.V., de Ruiter, H., Fanti, R., Morganti, R., Parma, P., 1990, ApJ 354, 98
- Burns, J.O., 1986, in: Henriksen R.N. (ed.), in: Jets from Stars and Galaxies, Can. J. Phys. 64, 373
- Cavaliere, A., Fusco-Femiano, R., 1981, A&A 100, 194
- De Vaucouleurs, G., de Vaucouleurs, A., Corwin, H.G. Jr., Buta, R.J., Paturel, P., Fouqué, P., 1991, in: Third Reference Catalogue of Bright Galaxies, Springer, New York
- Donnelly, H.R., Faber, S.M., O'Connell, R.M., 1990, ApJ 354, 52
- Fabbiano, G., 1989, Ann. Rev. A. Ap. 27, 87
- Fanti, R., 1984, in: Clusters and Groups of Galaxies, eds. F. Mardirossian, G. Giuricin & M. Mezzetti, Reidel P.C., Dordrecht, p. 185
- Fanti, R., Fanti, C., de Ruiter, H.R., Parma, P., 1986, A&AS 65, 145
- Feretti, L., Spazzoli, O., Gioia, I.M., Giovannini, G., Gregorini, L., 1990, A&A 233, 325
- Feretti, L., Perola, G.C., Fanti, R., 1992, A&A 265, 9
- Feretti, L., Fanti, R., Parma, P., Massaglia, S., Trussoni, E., Brinkmann, W., 1995, A&A 298, 699
- Fraix-Burnet, D., Golonbek, D., Macchetto, F.D., 1991, AJ 102, 562
- Impey, C.D., Wynn-Williams, C.G., Becklin, E.E., 1990, ApJ 356, 62
- Lynden-Bell, D., Faber, S.M., Burstein, D., Davies, R.L., Dressler, A., Terlevich, R.J., Wegner, G., 1988, ApJ 326, 19

- Makishima, K., Fujimoto, R., Ishisaki, Y., Kii, T., Loewenstein, M., Mushotzky, R., Serlemitsos, P., Sonobe, T., Tashiro, M., Yaqoob, T., 1994, PASJ 46, L77
- Massaglia, S., Trussoni, E., Caucino, S., Fanti, R., Feretti, L., Parma, P., Brinkmann W., 1996, A&A 309, 75
- Morganti, R., Fanti, C., Fanti, R., Parma, P., de Ruiter, H.R., 1987 A&A 183, 203
- Morganti, R., Fanti, R., Gioia, I.M., Harris, D.E., Parma, P., de Ruiter, H., 1988, A&A 189, 11
- Morganti, R., Ulrich, M.H., Tadhunter, C.N., 1992, MNRAS 254, 546
- Mulchaey, J.S., Davis, D.S., Mushotzky, R.F., Burstein, D., 1993, ApJ 404, L9
- Parma, P., Fanti, C., Fanti, R., Morganti, R., de Ruiter, H.R., 1987, A&A 181, 244
- Pfeffermann, E., Briel, U.G., Hippmann, H., et al., 1987, Proc. Society for Photo-Optical Instrumentation Engineers (SPIE) 733, 519
- Ponman, T.J., Bertram, D., 1993, Nat 363, 51
- Ponman, J.J., Allan, D.J., Jones, L.R., et al., 1994, Nat 369, 462
- Raymond, J.C., Smith, B.W., 1977, ApJS 35, 419
- Sarazin, C.L., 1986, Rev. Mod. Phys. 58, 1
- Strom, R.G., Fanti, R., Parma, P., Ekers, R.D., 1983 A&A 122, 305
- Trümper, J., 1983, Adv. Space Res. 2, 241
- Worrall, D.M., Birkinshaw, M., 1994, ApJ 427, 134
- Zimmermann, H.U., Becker, W., Belloni, T., Döbereiner, S., Izzo, C., Kahabka, P., Schwentker, O., 1995, EXSAS User's Guide, ed. 5, MPE Report n. 257